arXiv:0811.1528v1 [cond-mat.stat-mech] 10 Nov 2008

Numerical Evidence for the Haldane Conjecture

B. Allés[a], A. Papa[b]
[a] *INFN Sezione di Pisa, Pisa, Italy*
[b] *Dipartimento di Fisica, Università della Calabria and INFN Gruppo Collegato di Cosenza, Arcavacata di Rende (Cosenza), Italy*

The Haldane conjecture, when applied to the Heisenberg O(3) model with a θ term in two dimensions, states that the correlation length ξ diverges when θ approaches π. To verify this conjecture we have numerically simulated the model at imaginary θ and then analytically continued the results to real θ. We have obtained that the value where the model should become critical is $\theta = 3.10(5)$ in agreement with the expectation.

I. INTRODUCTION

It has been shown by Haldane that, depending on the value of the spin σ, the corresponding one dimensional antiferromagnetic chains of quantum spins present two kinds of large distance behavior. If σ is half–integer, they have a power law correlation function. Instead for integer spins they lie in a disordered phase and present an exponentially falling correlation function [1,2]. These results were obtained in the limit of large σ.

The generalization of the above behavior for all values (large or small) of the spin σ is called Haldane conjecture. This conjecture has been widely studied. Actually a partial result had already been proved for $\sigma = \frac{1}{2}$ in [3], while for all half–integer spins it was shown to be correct in [4]. Moreover, the analytic proof for spin $\sigma = 1$ was given in [5].

On the other hand there are indications [2,6,7] that the one dimensional antiferromagnetic chain of quantum spins σ shares the same large distance physical properties of the two dimensional O(3) nonlinear sigma model for classical spins with a θ term for $\theta = 2\pi\sigma$. This equivalence would imply that while the ground state of the two dimensional O(3) nonlinear sigma model at vanishing θ must display no long–range order and only short–range spin correlations, the model at $\theta = \pi$ should be critical. The first result is well–known, both analytically [8] and numerically [9]. However the large distance behavior of the correlation function of the model in the second case is a not so clearly settled question.

The two dimensional O(3) nonlinear sigma model is a valuable representation of several types of physical problems. Apart from the one dimensional quantum spin chains, in condensed matter physics it may describe the quantum Hall effect as well as being useful to understand superconductivity [10]. In particle physics it has in common with nonabelian gauge theories some important properties such as instantons, asymptotic freedom (criticality at zero temperature), a θ term, spontaneous generation of mass, etc.

Two recent numerical calculations of the partition function for the O(3) model in the presence of a θ term [11,12] suggest that the theory undergoes a second order phase transition at $\theta = \pi$ although the two analyses disagree about the universality class. Indeed the analysis of Bietenholz et al. [11] confirms the critical exponents of the Wess–Zumino–Novikov–Witten model at topological coupling $k = 1$ as predicted by Zamolodchikov et al. [7], while the numerical study of Azcoiti et al. [12] yields a set of continuously varying critical exponents.

In this work we introduce a direct numerical method to verify the Haldane conjecture for the two dimensional O(3) nonlinear sigma model at nonzero θ. The idea is to perform a Monte Carlo simulation to calculate the correlation length ξ on the lattice as a function of the θ parameter and to show that it diverges at a precise value of θ, called $\theta_{\rm end}$, which, following Haldane, should be $\theta_{\rm end} = \pi$.

Due to the (suppossed) divergence of the correlation length at $\theta_{\rm end}$, a direct simulation would become impracticable as it would require exponentially large lattice sizes. Moreover the Boltzmann weight in the partition function becomes complex for real θ and consequently it loses its probability meaning, thus precluding the importance sampling of Monte Carlo methods. We overcome these two difficulties by simulating the theory at imaginary θ (where ξ turns out to be small enough to allow the use of moderate lattice sizes) and analytically continuing the results to the real θ values. To this end we introduce a new fast cluster algorithm that works for imaginary nonzero theta. This work is an extended version of the paper appeared in [13].

In the next section we shall discuss the formulation of the model on the lattice and the corresponding lattice definition of the θ term and its meaning. The method to calculate the θ term is introduced in Section III. The new cluster algorithm expressly devised for the present work shall be described in Section IV. The results and corresponding plots are displayed in Section V. We end the paper with some conclusive comments in Section VI.

II. LATTICE IMPLEMENTATION AND NOTATION

The Boltzmann weight of the partition function in our simulations was $\exp(-S)$ with

$$\begin{aligned} S &= A - i\theta Q \ , \\ A &\equiv -\beta \sum_{x,\mu} \vec{\phi}(x) \cdot \vec{\phi}(x+\widehat{\mu}) \ , \end{aligned} \tag{1}$$

where the sum is extended over all lattice sites x and directions $\mu = 1, 2$. The factor β is the inverse temperature (in units of the spin coupling), Q is the total topological charge or winding number of the configuration (see later) and $\vec{\phi}(x)$ is a 3–component unit vector that represents the dynamical variable, a classical spin, at the site x. We have used a square lattice of lateral size L with periodic boundary conditions.

In the limit where the lattice spacing a vanishes (keeping $L \cdot a$ fixed), the above expression for A becomes the action of the classical field theory defined on a continuum two dimensional plane

$$A \stackrel{a\to 0}{\longrightarrow} \frac{\beta}{2} \int \left(\partial_\mu \vec{\phi}(x)\right)^2 \, \mathrm{d}^2 x \ , \tag{2}$$

together with the condition $\vec{\phi}(x)^2 = 1$.

In Fig. 1 we show a stereographic projection that defines an instanton configuration on the O(3) nonlinear sigma model. The two dimensional plane is shown where the configuration of spins lies. There is a unit sphere resting on the origin of the plane. One can draw straight lines that join the north pole N of the sphere with an arbitrary point F on the plane. One such a line pierces the sphere surface at point P. The unit vector that begins at the center C of the sphere and points to P is the value of the spin vector $\vec{\phi}(F)$ to be assigned at the point F of the plane. This construction defines a configuration called instanton and its analytical expression is the following (the lattice has been replaced by a continuum by sending $a \to 0$ as above, furthermore polar coordinates r and φ are used to locate the position of the spin variable)

$$\vec{\phi}(r,\varphi) = \left(\frac{4r\cos\varphi}{r^2+4}, \ \frac{4r\sin\varphi}{r^2+4}, \ \frac{r^2-4}{r^2+4} \right) \ . \tag{3}$$

In particular, notice that all spins at infinity are identified with the same value $\vec{\phi}(r=\infty,\varphi) = (0,0,1)$. Then spins slowly rotate while approaching $r = 0$ until becoming $\vec{\phi}(r=0,\varphi) = (0,0,-1)$ at the origin.

The spin value in Eq.(3) is a solution of the classical field equations associated to the action Eq.(2).

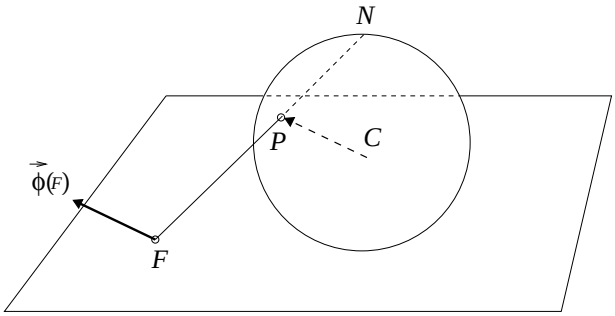

FIG. 1. A stereographic projection defines an instanton on the two dimensional O(3) nonlinear sigma model.

The main feature of instanton configurations is that the set of all spin vectors describes a complete winding of the sphere, as it is obvious in the example shown above. This winding can be calculated by the integral [14] (valid in the continuum two dimensional plane)

$$\begin{aligned} Q &= \int \mathrm{d}^2 x \, Q(x) \ , \\ Q(x) &\equiv \frac{1}{8\pi} \epsilon^{\mu\nu} \epsilon_{bcd} \phi^b(x) \partial_\mu \phi^c(x) \partial_\nu \phi^d(x) \ , \end{aligned} \tag{4}$$

where Q is called topological charge or winding number and $Q(x)$ is the topological charge density. Spatial indices μ, ν and O(3) vector indices b, c, d are summed up. For the instanton of Eq.(3) it yields -1. There are however many more instantonic configurations, besides that shown in Fig. 1 and in general Q takes any positive, negative or null integer value, depending on how many times and in what direction the whole set of spins covers the unit sphere.

The second main property is that instanton configurations carry a finite amount of energy (the operator A in Eq.(2) takes on a finite value) even when the lattice size L diverges.

In the Monte Carlo simulations we have used two different definitions of $Q(x)$. The first one [15]

$$Q^{(1)}(x) \equiv \frac{1}{32\pi}\epsilon^{\mu\nu}\epsilon_{bcd}\phi^b(x)\Big(\phi^c(x+\widehat{\mu}) - \phi^c(x-\widehat{\mu})\Big) \cdot \Big(\phi^d(x+\widehat{\nu}) - \phi^d(x-\widehat{\nu})\Big) \,, \tag{5}$$

is a symmetrical discretization of the expression for $Q(x)$ in Eq.(4) and is usually called "naive" definition. The corresponding winding number is $Q^{(1)} = \sum_x Q^{(1)}(x)$.

The second lattice expression that we used in our simulations is defined on triangles (not on single sites). Every plaquette of a square lattice can be cut through a diagonal into two triangles. If we call $\vec{\phi}_1$, $\vec{\phi}_2$ and $\vec{\phi}_3$ the fields at the sites of the three vertices (numbered counterclockwise) of one of these triangles, then the fraction of spherical angle subtended by these fields is $Q^{(2)}(\triangle)$ and it satisfies [16]

$$\exp\Big(2\pi i Q^{(2)}(\triangle)\Big) = \frac{1}{\rho}\Big(1 + \vec{\phi}_1\cdot\vec{\phi}_2 + \vec{\phi}_2\cdot\vec{\phi}_3 + \vec{\phi}_3\cdot\vec{\phi}_1 + i\vec{\phi}_1\cdot\Big(\vec{\phi}_2\times\vec{\phi}_3\Big)\Big) \,, \tag{6}$$

where $\rho^2 \equiv 2(1+\vec{\phi}_1\cdot\vec{\phi}_2)(1+\vec{\phi}_2\cdot\vec{\phi}_3)(1+\vec{\phi}_3\cdot\vec{\phi}_1)$ and $Q^{(2)}(\triangle) \in [-\frac{1}{2}, +\frac{1}{2}]$. The above conditions uniquely determine the portion of spherical angle subtended by $\vec{\phi}_1$, $\vec{\phi}_2$ and $\vec{\phi}_3$ and the sum of $Q^{(2)}(\triangle)$ over all triangles yields the so–called "geometrical" topological charge $Q^{(2)}$.

The two definitions $Q^{(1,2)}$ belong to the same universality class. In particular they both satisfy the limit

$$Q^{(1,2)}(x) \stackrel{a\to 0}{\longrightarrow} a^2 Q(x) \,, \tag{7}$$

where a is the lattice spacing.

III. EVALUATION OF Q

In general, a definition of Q on the lattice does not necessarily lead to integer values on a single configuration. To recover integer results for Q on ensembles of configurations that contain the same topological charge, we must renormalize this operator. The lattice and the continuum topological charges are related by [17]

$$Q^{(1,2)} = Z_Q^{(1,2)} Q \,, \tag{8}$$

$Z_Q^{(1,2)}$ being the corresponding renormalization constant. The origin of this constant can be traced back to the presence of statistical fluctuations in an otherwise smooth instantonic configuration. In general operators that reveal the topological charge Q of a configuration give wrong answers due to the disturbance caused by the presence of fluctuations.

The $Z_Q^{(1,2)}$ function depends only on the temperature β and is chosen in such a way not to depend on θ since the introduction of this term does not modify the structure of fluctuations in the model. Moreover it satisfies $0 < Z_Q^{(1,2)} \leq 1$ for all values of the lattice spacing [18,15].

$Z_Q^{(1,2)}$ can be calculated either in perturbation theory [17,18,15] or by a nonperturbative numerical method [19–21]. We have used the latter. In a nutshell it works in the following way: one measures $Q^{(1,2)}$ on an instantonic configuration (topological charge $Q = +1$) after heating it at a temperature β. From Eq.(8) this measurement yields $Z_Q^{(1,2)}$.

First of all an instanton with topological charge $+1$ is put by hand on the lattice. We used the solution [22]

$$\frac{\phi^1 + i\phi^3}{1-\phi^2} = \frac{x_1 - L/2 - i(x_2 - L/2)}{\lambda\, e^{i\pi/4}} \,, \tag{9}$$

where ϕ^b is the b–component of the field at site $x = (x_1, x_2)$, L is the size of the lattice and λ is the size of the instanton. This solution is the one shown in Eq.(3) after centering it in the middle of the lattice $(L/2, L/2)$, dilating it to the size λ (the size in Eq.(3) is $\lambda = 2$) and performing appropriate rotations both in x–space and O(3) space [23]. In order to work with a rather stable instanton (recall that single instantons on the lattice are only metastable solutions of the equations of motion on a torus) it is convenient to choose $\lambda \lesssim 0.15\, L$ and $\lambda \gtrsim 8$ [21]. We took $\lambda = 16$ on a $L = 120$ lattice.

Then 100 updating steps are applied (we used the Heat–Bath algorithm [24] on the conventional O(3) nonlinear sigma model without a θ term since the renormalization constant to be used in Eq.(8) does not depend on θ). After every Heat–Bath step the value of $Q^{(1,2)}$ is measured and, in order to monitor the instantonic contents and check that it is not varied after the updating step, $Q^{(1,2)}$ is measured again after 6 relaxation hits applied on a separate copy of the running configuration. The complete history of 100 Heat–Bath updating steps and related measurements of $Q^{(1,2)}$ is called a *trajectory*. In the calculation of $Z_Q^{(1)}$ we used $4 \cdot 10^4$ trajectories at $\beta = 1.5$ and 1.6 and 10^4 trajectories for $\beta = 1.7$ and 1.75. The average of $Q^{(1,2)}$ on all trajectories, as long as their topological charge remained equal to $+1$, yielded $Z_Q^{(1,2)}$.

The O(3) nonlinear sigma model develops an infrared divergence in its instanton size distribution [25,20]. This divergence facilitates the copious creation of new instantonic objects at every updating step, thus modifying the total topological charge of the configuration. For this reason the relaxation test is extremely important.

As a relaxation method we used the so–called cooling [26]. It sweeps through the whole lattice and modifies one by one every single spin variable in order to locally minimize the energy of the relaxed configuration. Actually many variants of the cooling method exist in the literature but in practice all of them act analogously [27].

The above nonperturbative method is summarized by the expression

$$Z_Q^{(1,2)} = \frac{\int_{1-\mathrm{instanton}} \mathcal{D}\vec{\phi}\, Q^{(1,2)}\, \exp(-A)}{\int_{1-\mathrm{instanton}} \mathcal{D}\vec{\phi}\, \exp(-A)}\,, \tag{10}$$

where $\mathcal{D}\vec{\phi}$ stands for the measure

$$\prod_x \left(\delta(\vec{\phi}(x)^2 - 1) \prod_b \mathrm{d}\phi^b(x) \right) \tag{11}$$

and $\int_{1-\mathrm{instanton}}$ means that the integration is extended over all configurations (fluctuations) that preserve the background of one instanton. Since the geometrical charge $Q^{(2)}$ is $+1$ till the background configuration is one instanton, the expression (10) yields $Z_Q^{(2)} = 1$ for all β [28]. This result derives from the fact that fluctuations, viewed as local large (positive or negative) values of the spherical angle in some spherical triangles, cancel out when summing up all individual contributions $Q^{(2)}(\triangle)$.

The determination of $Z_Q^{(1)}$ is not so trivial and an example of such an evaluation is shown in Fig. 2. Measures of $Q^{(1)}$ on configurations that have topological charge $+1$ attain to a plateau (in general after a few Heat–Bath steps) and stay on it for the rest of the updating steps. The height of this plateau is the value of $Z_Q^{(1)}$. In Table 1 the results for $Z_Q^{(1)}$ at the values of β used in the present work are given.

Table 1. $Z_Q^{(1)}$ and θ_{end} for the topological charge $Q^{(1)}$.

β	$\left(\overline{\theta}_{\mathrm{end}}\right)^2$	$Z_Q^{(1)}$	χ^2/d.o.f.	θ_{end}
1.5	111(5)	0.285(9)	0.90	3.00(12)
1.6	94(5)	0.325(6)	0.45	3.15(10)
1.7	67(3)	0.380(6)	1.04	3.11(9)
1.75	56(3)	0.412(5)	0.68	3.08(9)

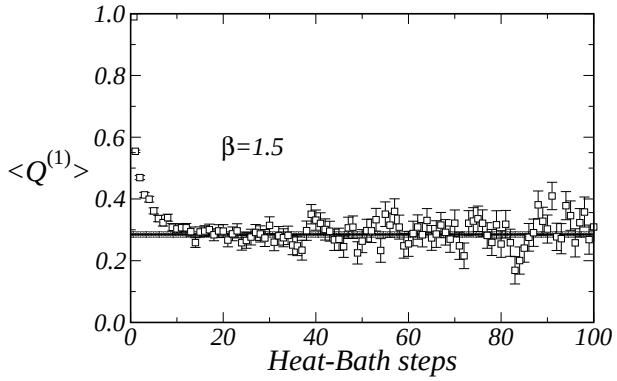

FIG. 2. Data for $\langle Q^{(1)} \rangle$ start at +1 at the 0–th Heat–Bath step and then they go down until reaching a plateau. The height of the horizontal line and grey band are the value and error respectively of $Z_Q^{(1)}(\beta = 1.5)$.

In Fig. 3 an histogram of the distribution of topological charge $Q^{(1)}$ is shown. It has been produced from the data of $Q^{(1)}$ obtained during the calculation of $Z_Q^{(1)}$ at $\beta = 1.5$ and contains 70 bins within the interval $Q^{(1)} \in [-4, +4]$. For each trajectory in the calculation of $Z_Q^{(1)}$ we obtained the average of $Q^{(1)}$ over the steps that come after the onset of the plateau (from Fig. 2 this happens at about the 15th step for $\beta = 1.5$) and for which the cooling test gave a background topological charge +1. The histogram of Fig. 3 displays the distribution of these averages. Each of the above averages turns out to be an uncorrelated estimate of $Z_Q^{(1)}$. The thick vertical line is the value of $Z_Q^{(1)}$, 0.285(9). Actually the error in the evaluation of $Z_Q^{(1)}$ was determined by using this kind of plot. Indeed, it was extracted by usual gaussian analysis on the histogram.

Recall that the number of trajectories for $\beta = 1.5$ was 40000. However the area of the histogram in Fig. 3 is much less than 40000. This is due to the fact that in many trajectories the background charge is no longer +1 already at the beginning of the plateau. In such cases, the whole trajectory was discarded. The area under the histogram in Fig. 3 is about 6700. The small ratio 6700/40000 gives an idea of the frequent creation of new instantonic objects that modify the background topological charge.

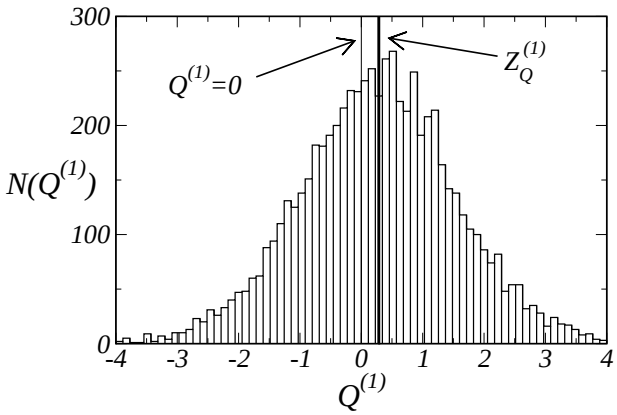

FIG. 3. Histogram displaying the distribution of naive topological charge at $\beta = 1.5$ starting from an initial configuration with background topological charge +1. Observe the shift of the gaussian–like distribution towards positive values of $Q^{(1)}$ (a vertical thin line indicates the zero value and a thicker line the result of $Z_Q^{(1)}$).

The renormalization of the topological charge brings about a relevant consequence for our study: the θ parameter that appears in the expression of the Hamiltonian used in the computer program during the simulations in general is *not* equal to the true physical θ parameter. Henceforth we shall call $\overline{\theta}$ the parameter that appears in the simulation program and the relation among the two parameters is $\theta = \overline{\theta} Z_Q^{(1,2)}$. The value of $\overline{\theta}$ where the correlation length diverges will be called $\overline{\theta}_{\rm end}$. Since $Z_Q^{(2)} = 1$, it is clear that this distinction among theta parameters is irrelevant for the geometrical charge $Q^{(2)}$.

We have simulated the model at several temperatures β and parameters $\overline{\theta}$ for the two topological charge operators $Q^{(1)}$ and $Q^{(2)}$ in order to show that our results are independent of the operator chosen for the simulation. Moreover, for the case of the naive topological charge $Q^{(1)}$, we have introduced a very fast cluster algorithm. Instead, for the geometrical charge $Q^{(2)}$ a rather slow Metropolis–like algorithm has been used. Actually the cluster algorithm for the naive charge was so efficient that it took much less computer time to investigate this charge than the geometrical one even though the naive charge required the extra calculation of $Z_Q^{(1)}$ by a separate out–of–equilibrium simulation for each temperature β as described above.

IV. CLUSTER ALGORITHM FOR IMAGINARY θ

Although the use of the topological charge density $Q^{(1)}$ requires the knowledge of a renormalization constant, it brings about the advantage that the Hamiltonian in (1) can be simulated on the lattice by use of a fast cluster algorithm when $\overline{\theta}$ is imaginary.

Let us briefly describe the main characteristics of the new cluster algorithm expressly devised for the present work. The first part of an updating step with the usual Wolff algorithm [29] for the standard O(3) sigma model without a θ term consists in choosing a random unit vector $\vec{r}$ in such a way that every dynamical field can be split in a component parallel to $\vec{r}$ and the rest, $\vec{\phi}(x) = \left(\vec{\phi}(x)\cdot\vec{r}\right)\vec{r} + \vec{\phi}_\perp(x)$, where $\vec{\phi}_\perp(x)$ denotes the part of $\vec{\phi}(x)$ orthogonal to $\vec{r}$. Then the signs of $\left(\vec{\phi}(x)\cdot\vec{r}\right)$ for all x are updated à la Swendsen–Wang as in the Ising model [30].

By introducing the above separation for $\vec{\phi}(x)$ in the expression (5) and recalling elementary properties of determinants in three dimensional vector spaces, we can rewrite it as

$$\begin{aligned} Q^{(1)}(x) = & \\ & \frac{1}{16\pi}\Big\{ \left(\vec{\phi}(x)\cdot\vec{r}\right)\left(d_{1,2}+d_{-1,-2}+d_{2,-1}+d_{-2,1}\right) \\ & \quad + \left(\vec{\phi}(x+\widehat{1}\,)\cdot\vec{r}\right)\left(d_{0,-2}-d_{0,2}\right) \\ & \quad + \left(\vec{\phi}(x-\widehat{1}\,)\cdot\vec{r}\right)\left(d_{0,2}-d_{0,-2}\right) \\ & \quad + \left(\vec{\phi}(x+\widehat{2}\,)\cdot\vec{r}\right)\left(d_{0,1}-d_{0,-1}\right) \\ & \quad + \left(\vec{\phi}(x-\widehat{2}\,)\cdot\vec{r}\right)\left(d_{0,-1}-d_{0,1}\right)\Big\}\,, \end{aligned} \tag{12}$$

where $x \pm \widehat{1}$ means the site at the position one step forward (backward) in the direction "1" starting from site x and the notation $d_{i,j}$ stands for the 3×3 determinant

$$d_{i,j} \equiv \det\begin{pmatrix} r^1 & r^2 & r^3 \\ \phi^1(x+\widehat{i}\,) & \phi^2(x+\widehat{i}\,) & \phi^3(x+\widehat{i}\,) \\ \phi^1(x+\widehat{j}\,) & \phi^2(x+\widehat{j}\,) & \phi^3(x+\widehat{j}\,) \end{pmatrix}\,. \tag{13}$$

In this fashion the theory at each updating step looks like an Ising model in the bosom of an external local magnetic field $h(x)$ because the expression in Eq.(12) is linear in $\left(\vec{\phi}\cdot\vec{r}\right)$. The value of this field varies at each updating and accordingly it must be recalculated after every step. Recall that all Monte Carlo simulations have been performed with an imaginary parameter $\overline{\theta} = +i\overline{\vartheta}$, ($\overline{\vartheta}\in\mathbb{R}$). By gathering all contributions of the type shown in Eq.(12) that contain $\left(\vec{\phi}(x)\cdot\vec{r}\right)$ at site x one can readily derive the effective magnetic field at this site,

$$\begin{aligned} h(x) = & -\frac{\overline{\vartheta}}{16\pi}|\vec{\phi}(x)\cdot\vec{r}\,|\Big(d_{1,2}+d_{-1,-2}+d_{2,-1}+d_{-2,1} \\ & + \quad d_{-1,-1-2}+d_{-1+2,-1}+d_{1,1+2}+d_{1-2,1} \\ & + \quad d_{2,2-1}+d_{2+1,2}+d_{-2,-2+1}+d_{-2-1,-2}\Big)\,. \end{aligned} \tag{14}$$

$d_{i+k,j}$ (and analogous terms in (14)) are the straightforward generalization of the above definition (13) when the site is obtained by shifting two steps from the original position x, the first in the direction $\widehat{i}$ and the second in the direction $\widehat{k}$.

Hence the last step in the updating consists in applying to the above expressions an algorithm valid for the Ising model in presence of a magnetic field. In the literature there are two such algorithms, the Lauwers–Rittenberg [31] and the Wang [32,33] methods. After testing their perfomances and comparing the corresponding decorrelation times with the usual Metropolis [34], Heat–Bath [24] and overHeat–Bath [35], we decided on the Wang algorithm. It consists in placing the magnetic field on an extra, fictitious site (called ghost site or ghost spin) that couples to every Ising spin through the value of $h(x)$. Using this coupling on the same footing as all other terms in the action, the Fortuin–Kasteleyn clusters [36] are created by using the Hoshen–Kopelman algorithm [37] and then updated with the usual $\frac{1}{2}$ probability. The only distinctive feature of the presence of a ghost spin is that the cluster that contains it does not flip.

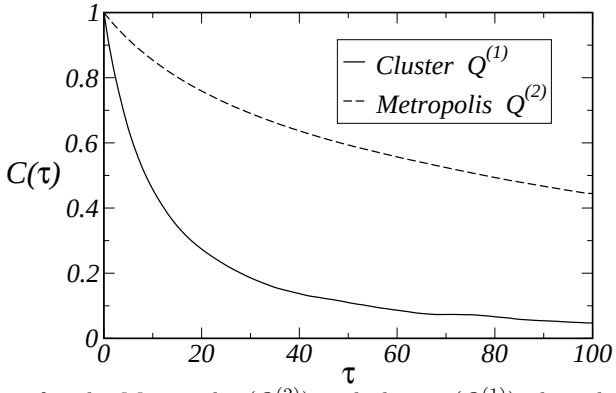

FIG. 4. Autocorrelation functions for the Metropolis ($Q^{(2)}$) and cluster ($Q^{(1)}$) algorithms as a function of the "updating time" τ which has a discrete ticking at each updating step.

Following the proof given in [29], it can be seen that our algorithm also satisfies the detailed balance property.
To generate the initial random unit vector $\vec{r}$ the method proposed in Ref. [38] was used.
In Fig. 4 we show the autocorrelation functions

$$C(\tau) \equiv \frac{\langle E_0 E_\tau \rangle - \langle E \rangle^2}{\langle E^2 \rangle - \langle E \rangle^2} \,, \tag{15}$$

calculated from the measures of the energy operator $E \equiv \vec{\phi}(x) \cdot \vec{\phi}(x+\widehat{\mu})$ (not summed over μ), for the two algorithms: Metropolis when the $Q^{(2)}$ operator is used and the above–described cluster algorithm for $Q^{(1)}$. E_τ indicates the τ–th measurement. In both cases $\beta = 1.5$ and $L = 120$. The theta parameter was $\overline{\vartheta} = 10$ for $Q^{(1)}$ and $\vartheta = 2.85$ for $Q^{(2)}$ (note that this choice was dictated by the condition $\theta = Z_Q^{(1)}(\beta = 1.5)\overline{\theta}$). The plot clearly exhibits the major efficiency of the cluster algorithm.

V. RESULTS

As the ground state of the model is a triplet [39], we studied the correlation functions of operators having one O(3) index. We measured the correlation of the two operators

$$\overrightarrow{\mathcal{O}}_1(x) \equiv \vec{\phi}(x) \,, \qquad \overrightarrow{\mathcal{O}}_2(x) \equiv \vec{\phi}(x) \times \vec{\phi}(x+\widehat{1}\,) \,. \tag{16}$$

Firstly we calculated the corresponding wall operators by averaging over the x_1 coordinate

$$\overrightarrow{\mathcal{W}}_1(x_2) \equiv \frac{1}{L} \sum_{x_1} \overrightarrow{\mathcal{O}}_1(x) \,, \; \overrightarrow{\mathcal{W}}_2(x_2) \equiv \frac{1}{L} \sum_{x_1} \overrightarrow{\mathcal{O}}_2(x) \,. \tag{17}$$

In order to extract the correct correlation length and to clean its signal from any mixture with higher eigenvalues of the Transfer Matrix, we used the variational method of Ref. [40], where ξ is obtained from the exponential decay of the largest eigenvalue of the correlation matrix

$$\langle \overrightarrow{\mathcal{W}}_i(x_2) \cdot \overrightarrow{\mathcal{W}}_j(0) \rangle - \langle \overrightarrow{\mathcal{W}}_i \rangle \cdot \langle \overrightarrow{\mathcal{W}}_j \rangle \ . \tag{18}$$

No improved estimators [41] were used since the operators in (17) contain too many fields $\vec{\phi}$ and this fact leads to intractable sums over clusters [42].

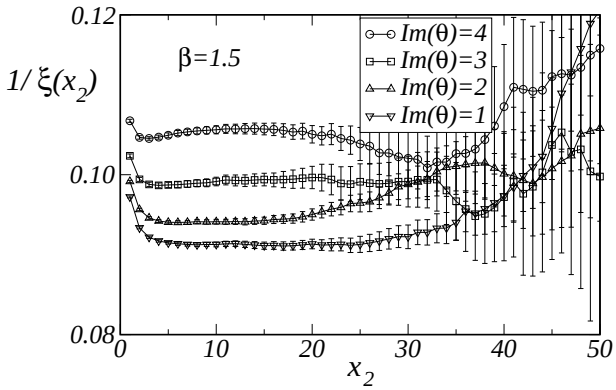

FIG. 5. Determination of ξ at $\beta = 1.5$ for four values of $Im(\theta) \equiv \vartheta$ for the case of the $Q^{(1)}$ operator. Lines are drawn to guide the eye.

In Fig. 5 the method that we followed to extract ξ is illustrated with four examples. The exponent of the fall–off of the largest eigenvalue $\alpha_{\max}$ of the correlation matrix, Eq.(18), is plotted against the distance x_2. For each x_2 it was extracted by comparing the expression

$$\frac{\alpha_{\max}(x_2)}{\alpha_{\max}(x_2 - 1)} \ , \tag{19}$$

with the theoretical behavior (L is the lattice size)

$$\frac{\cosh\Big((x_2 - L/2)/\xi \Big)}{\cosh\Big((x_2 - 1 - L/2)/\xi \Big)} \ , \tag{20}$$

and its error was determined by jackknife. An approximate plateau is clearly identified at moderate distances. The definite values of ξ and its error were chosen self–consistently at $x_2 = 2\xi$.

For each β we calculated ξ from Monte Carlo simulations at several imaginary values of $\overline{\theta}$ for both $Q^{(1)}$ and $Q^{(2)}$. The set of results for a given β were then analytically continued from imaginary $\overline{\theta}$ to the real $\overline{\theta}$ axis by an usual procedure of numerical extrapolation. In the extrapolation we avoided using a trial function dictated by some theoretical argument, like for instance $1/\xi = c_1 \left(c_2 - \overline{\theta}^2 \right)^{2/3}$ which is, up to logarithmic corrections, the Renormalization Group prediction [43], because such an analytic form implicitly assumes the vanishing of $1/\xi$ at a precise value of $\overline{\theta}$ (not to say that it is supposed to be accurate only in a close neighborhood of its zero, $\overline{\theta} = \sqrt{c_2}$). Instead we made the extrapolations by using polynomials in $\overline{\theta}^2$ and ratios of such polynomials. These functional forms are indeed both simple and very general and they leave room for any possible behavior in $\overline{\theta}$.

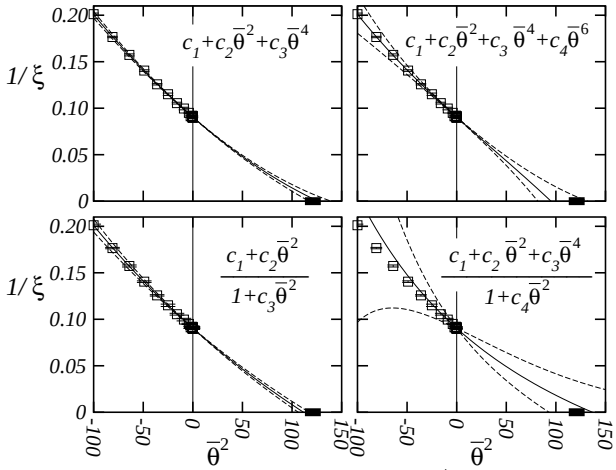

FIG. 6. Four extrapolations for the same set of Monte Carlo data of $1/\xi$. The scale in the axes is the same for the four windows. Data were extracted from simulations at $\beta = 1.5$ and using the $Q^{(1)}$ operator for the topological charge. The horizontal black bar is placed at the value of $\overline{\theta}$ where the Haldane conjecture predicts a critical behavior. Each continuous line is the result of the extrapolation and the dashed lines enclose the boundary of its error.

A. Results for $Q^{(1)}$

$2 \cdot 10^5$ decorrelated propagators were measured for all values of $\overline{\theta}$ at each β. They were obtained after separating consecutive configurations by a combination of one Heat–Bath, two overHeat–Bath and one cluster updatings. The values obtained for $1/\xi$ at $\beta = 1.5$ with their error bars are the squares in Fig. 6. In this figure four different extrapolations are shown (the extrapolation functional forms are displayed). The Haldane conjecture predicts that $1/\xi$ vanishes at $\left(\pi/Z_Q^{(1)}(\beta = 1.5)\right)^2$. This value is indicated by the small horizontal shadowed bar on the $\overline{\theta}^2$ axis (its horizontal width arises from the error in the evaluation of $Z_Q^{(1)}(\beta = 1.5)$, see Table 1). From Fig. 6 it seems clear that all analytic continuations are in fair agreement among themselves and with the Haldane conjecture. We emphasize that no prejudices about the possible zeroes were included in the extrapolating functions.

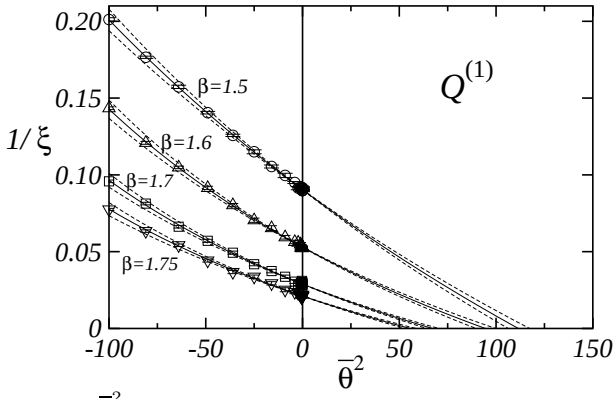

FIG. 7. Behavior of $1/\xi$ as a function of $\overline{\theta}^2$. Circles ($\beta = 1.5$), up triangles ($\beta = 1.6$), squares ($\beta = 1.7$) and down triangles ($\beta = 1.75$) are the data from the simulation at imaginary $\overline{\theta}$ ($\overline{\theta}^2 < 0$) by using the $Q^{(1)}$ lattice topological charge. Meaning of continuous and dashed lines as in Fig. 6.

Four values of β were studied in the case of $Q^{(1)}$: $\beta = 1.5$, 1.6, 1.7 and 1.75. The respective sets of Monte Carlo data for $1/\xi$ are shown in Fig. 7 as circles, up triangles, squares and down triangles. The lattice sizes were 120, 180, 340 and 470 respectively. The extrapolations in this figure were done by using the functional form $(c_1 + c_2\,\overline{\theta}^2)/(1 + c_3\,\overline{\theta}^2)$

since it was the one that produced the value of the statistical χ^2 test closer to 1 for all four β's (the values for χ^2/d.o.f. are listed in Table 1).

The results of the analytic continuations are given in Table 1. The physical value of θ where the theory becomes critical is given by $\theta_{\rm end} = \overline{\theta}_{\rm end} Z_Q^{(1)}$. The numbers in the last column are in good agreement with the prediction that criticality is achieved when θ equals π. Other functional forms used for the extrapolations led to similar results although in some cases the χ^2 test was far from unity and hence the related extrapolation seemed statistically unlikely (see for instance the $(c_1 + c_2\,\overline{\theta}^2 + c_3\,\overline{\theta}^4)/(1 + c_4\,\overline{\theta}^2)$ case in Fig. 6).

The lattice sizes were chosen large enough to meet at $\overline{\theta} = 0$ the condition $L/\xi \gtrsim 10$ (to be specific, these ratios were 10.8, 9.5, 9.8 and 9.9 for $\beta = 1.5$, 1.6, 1.7 and 1.75 respectively). Once this inequality holds at $\overline{\theta} = 0$, it is amply realized at the values of $\overline{\theta}$ where the simulations were performed as inferred from Fig. 7. This fact warrants the absence of significant finite size effects.

On the other hand, from the Monte Carlo values of ξ shown in Fig. 7 one can see that we simulated the model at correlation lengths that altogether satisfy $\xi > 5$ which is safely far from the strong coupling region (in this region the universality property loses its meaning and results may depend on the choice of operators used in the action).

B. Results for $Q^{(2)}$

In this case the usual Metropolis algorithm was used for updating. Observe that when the spin variable $\vec{\phi}(x)$ is updated, the θ term in Eq.(1) will contribute to the variation of the Hamiltonian only if the topological charge gets modified within the only six triangles that surround the site x. Such modifications occur only if some instantonic object rises or disappears in the area delimited by these six triangles. Such an event barely occurs on a such a small area and as a consequence prolonged decorrelations must separate consecutive measurements of any operator (see Fig. 4).

10^5 independent propagators, separated by 100 decorrelation updatings, were measured for each value of θ (recall that for $Q^{(2)}$ we have $\overline{\theta} = \theta$). We report data for only two values of β. Notice that the total statistics and the number of β values studied is evidently smaller here than in the previous subsection. As explained above, this is due to the use of a much less efficient updating algorithm.

Data are displayed in Fig. 8 as squares and triangles for $\beta = 1.5$ and 1.55 respectively. The corresponding lattice sizes were $L = 110$ and 150. The value of θ where Haldane predicted the vanishing of $1/\xi$ is indicated with an arrow, $\theta^2 = \pi^2$. Data near $\theta^2 = 0$ are very noisy. This is due to the relatively poor statistics obtained in the simulations with the operator $Q^{(2)}$.

The numerical results are given in Table 2. Comments similar to the $Q^{(1)}$ case apply to the extrapolations shown in the figure. From Fig. 8 the correlation lengths satisfy $\xi > 3$ which is still away from the strong coupling regime. Again the results are in fair agreement with the conjecture.

Table 2. $\theta_{\rm end}$ for the operator $Q^{(2)}$.

β	$\left(\overline{\theta}_{\rm end}\right)^2$	$Z_Q^{(2)}$	χ^2/d.o.f.	$\theta_{\rm end}$
1.5	10.4(1.0)	1.0	1.72	3.22(16)
1.55	9.7(1.0)	1.0	0.73	3.11(16)

By averaging all results for both topological charge operators and assuming gaussian errors we obtain that the model should become critical at $\theta_{\rm end} = 3.10(5)$. This is the chief result of our work.

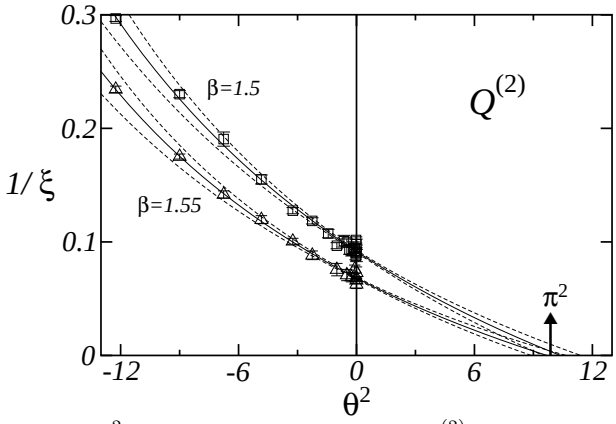

FIG. 8. Behavior of $1/\xi$ as a function of θ^2 for the geometrical charge $Q^{(2)}$. Squares ($\beta = 1.5$) and up triangles ($\beta = 1.55$). In this case $\theta = \overline{\theta}$ and the position of $\theta = \pi$ is marked. Meaning of continuous and dashed lines as in Fig. 6.

VI. CONCLUSIONS

We have simulated the O(3) nonlinear sigma model in two dimensions with an imaginary θ term at several values of the inverse temperature β. The correlation length was measured and extrapolated towards real θ. In all cases the extrapolation showed a divergence at a value of θ compatible with the Haldane conjecture $\theta = \pi$. Our result is $\theta = 3.10(5)$ which agrees within errors with the conjecture. This value seems very robust as it is independent of the topological charge density operator chosen for the simulation. In particular, an operator $Q^{(1)}$ that requires a nontrivial renormalization constant leads to the same conclusion than another operator (the geometrical charge $Q^{(2)}$) that does not renormalize.

A direct numerical study of the model at θ values which are both real and close to π is unfeasible. First of all at real θ the Hamiltonian becomes complex, thus preventing the importance sampling in Monte Carlo methods. Furthermore exponentially large lattice sizes would be required to avoid the severe finite size effects that would supervene in simulations performed close to the critical point $\theta = \pi$.

A new fast cluster algorithm was purposely introduced to simulate the theory with an imaginary θ term. It works for the operator $Q^{(1)}$.

A salient outcome of our work is the good performance of the analytic continuation from imaginary to real θ. No theoretical prejudices were assumed in the functional form used in the extrapolation and different functions led to comparable results (see Fig. 6).

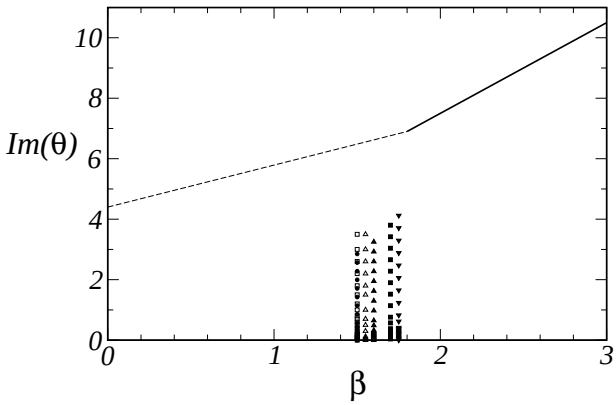

FIG. 9. Possible phase diagram in the $Im(\theta)$–β plane, ($Im(\theta) \equiv \vartheta$). The phase transition lines (continuous line is first order and dashed line is at most second order) are borrowed from Ref. [44]. Symbols are situated at the positions where single simulations were done. Filled (white) symbols mean simulations with $Q^{(1)}$ ($Q^{(2)}$) and the vertical sequences of data correspond, from left to right, to $\beta = 1.5$, 1.55, 1.6, 1.7 and 1.75. In this diagram extrapolations appear as going downwards starting from the Monte Carlo data points, hence they never touch the phase transition lines.

A key ingredient for the successful extrapolation was to have got data from simulations within a wide range of (imaginary) values of $\overline{\theta}$ for all β, ($\overline{\vartheta} \equiv -i\overline{\theta} \in [0, 10]$ when $Q^{(1)}$ was used and $\overline{\vartheta} = \vartheta \equiv -i\theta \in [0, 3.5]$ for $Q^{(2)}$, the difference of intervals being due to the effect of the nontrivial renormalization that must be applied to the former). We also noticed that at very large values of imaginary $\overline{\theta}$ the extraction of the correlation length becomes more imprecise since the kind of plateaux shown in Fig. 5 shrink making it difficult to decide the correct result for ξ and its error bar. This problem appears approximately at $\overline{\vartheta} \geq 15$ for the $Q^{(1)}$ charge density. Then, the method consists in taking data in a wide range of values of imaginary $\overline{\theta}$ (or θ) while staying not too far from the real axis in order to make the extrapolation sensitive to the real physics of the problem and in order to have wide enough plateaux which allow to easily extract the correlation length ξ.

Moreover our extrapolations did not cross any nonanalytical region in the phase diagram of the model. Indeed in Fig. 9 we show a schematic reproduction of the phase diagram that appears in Ref. [44]. The first order transitions lie on the continuous straight line while the dashed line indicates less singular transitions, at most second order. Our simulations were performed at the positions indicated by the symbols (same symbols than in Figs. 7 and 8; notice that this plot refers to the values of θ, not of $\overline{\theta}$, for both topological charge density definitions) and the corresponding analytic continuations proceed downwards, thus very far from any possible line of singular points.

For $\theta > \pi$ the model should acquire again a finite correlation length since the Hamiltonian is a periodic function of θ. However an analytical continuation could hardly display such a behavior beyond $\theta = \pi$ because of the nonanalyticity at that value of θ.

VII. ACKNOWLEDGEMENTS

It is a pleasure to thank Juan José Alonso for a critical reading of a draft of the paper. We are indebted to CINECA (Italy) for the use of their HPC system for part of our production runs.

---

[1] F. D. M. Haldane, Phys. Lett. **93A**, 464 (1983).
[2] F. D. M. Haldane, Phys. Rev. Lett. **50**, 1153 (1983).
[3] E. H. Lieb, T. Schultz and D. Mattis, Ann. Phys. (N.Y.) **16**, 407 (1961).
[4] I. Affleck and E. H. Lieb, Lett. Math. Phys. **12**, 57 (1986).
[5] I. Affleck, T. Kennedy, E. H. Lieb and H. Tasaki, Phys. Rev. Lett. **59**, 799 (1987).
[6] R. Shankar and N. Read, Nucl. Phys. **B336**, 457 (1990).
[7] A. B. Zamolodchikov and Al. B. Zamolodchikov, Nucl. Phys. **B379**, 602 (1992).
[8] P. Hasenfratz, M. Maggiore and F. Niedermayer, Phys. Lett. B **245**, 522 (1990).
[9] B. Allés, A. Buonanno and G. Cella, Nucl. Phys. **B500**, 513 (1997).
[10] E. Fradkin, "Field Theories of Condensed Matter Systems", (Addison–Wesley, Reading MA, 1991).
[11] W. Bietenholz, A. Pochinsky and U.–J. Wiese, Phys. Rev. Lett. **75**, 4524 (1995).
[12] V. Azcoiti, G. Di Carlo and A. Galante, Phys. Rev. Lett. **98**, 257203 (2007).
[13] B. Allés and A. Papa, Phys. Rev. D **77**, 056008 (2008).
[14] See for instance R. Rajaraman, "Solitons and Instantons", (North-Holland, Amsterdam, 1982).
[15] A. Di Giacomo, F. Farchioni, A. Papa and E. Vicari, Phys. Rev. D **46**, 4630 (1992).
[16] B. Berg and M. Lüscher, Nucl. Phys. **B190**, 412 (1981).
[17] M. Campostrini, A. Di Giacomo and H. Panagopoulos, Phys. Lett. B **212**, 206 (1988).
[18] B. Allés and E. Vicari, Phys. Lett. B **268**, 241 (1991).
[19] A. Di Giacomo and E. Vicari, Phys. Lett. B **275**, 429 (1992); B. Allés, M. Campostrini, A. Di Giacomo, Y. Gündüç and E. Vicari, Phys. Rev. D **48**, 2284 (1993).
[20] F. Farchioni and A. Papa, Nucl. Phys. **B431**, 686 (1994).
[21] B. Allés, M. Beccaria and F. Farchioni, Phys. Rev. D **54**, 1044 (1996).
[22] A. A. Belavin and A. M. Polyakov, JETP Lett. **22**, 245 (1975).
[23] A rotation of $\pi/4$ radians in x–space; another rotation of $\pi/2$ radians around the 1–axis in O(3) group space and a parity inversion in the O(3) space again on the resultant 3–axis (this last inversion allows to end up with a topological charge $Q = +1$ object).
[24] M. Creutz, Phys. Rev. D **21**, 2308 (1980).
[25] A. Jevicki, Nucl. Phys. **B127**, 125 (1977); C. Michael and P.S. Spencer, Phys. Rev. D **50**, 7570 (1994).
[26] M. Teper, Phys. Lett. B **171**, 81 (1986); B **171**, 86 (1986).

[27] See B. Allés, L. Cosmai, M. D'Elia and A. Papa, Phys. Rev. D **62**, 094507 (2000) and references therein.
[28] M. Lüscher, Commun. Math. Phys. **85**, 39 (1982).
[29] U. Wolff, Phys. Rev. Lett. **62**, 361 (1989).
[30] R. Swendsen and J.–S. Wang, Phys. Rev. Lett. **58**, 86 (1987).
[31] P. G. Lauwers and V. Rittenberg, Phys. Lett. B **233**, 197 (1989).
[32] J.–S. Wang, Physica A (Amsterdam) **161**, 249 (1989).
[33] I. Dimitrovic, P. Hasenfratz, J. Nager and F. Niedermayer, Nucl. Phys. **B350**, 893 (1991).
[34] N. Metropolis, A. Rosenbluth, M. Rosenbluth, A. Teller and E. Teller, J. Chem. Phys. **21**, 1087 (1953).
[35] R. Petronzio and E. Vicari, Phys. Lett. B **254**, 444 (1991).
[36] C. M. Fortuin and P. W. Kasteleyn, Physica (Amsterdam) **57**, 536 (1972).
[37] J. Hoshen and R. Kopelman, Phys. Rev. B **14**, 3438 (1976).
[38] F. Niedermayer, Phys. Lett. B **237**, 473 (1990).
[39] D. Controzzi and G. Mussardo, Phys. Rev. Lett. **92**, 021601 (2004); Phys. Lett. B **617**, 133 (2005); L. Campos Venuti, C. Degli Esposti Boschi, E. Ercolessi, F. Ortolani, G. Morandi, S. Pasini and M. Roncaglia, J. Stat. Mech. (2005) L02004.
[40] A. S. Kronfeld, Nucl. Phys. Proc. Suppl. **17**, 313 (1990); M. Lüscher and U. Wolff, Nucl. Phys. **B339**, 222 (1990).
[41] U. Wolff, Nucl. Phys. Proc. Suppl. **17**, 93 (1990).
[42] Had we decided to make use of improved estimators (at least for the two–point correlation functions), the only algorithm that would have allowed us to use them is the Wang algorithm [32]; if instead we had decided on the Lauwers–Rittenberg method [31], then the calculation of improved estimators would have become again intractable even for simple two–point correlators $\langle\vec{\phi}(x)\cdot\vec{\phi}(y)\rangle$. In fact, in such a case the expression of the estimator when x, y belong to different clusters (say C_x and C_y) does not vanish but comes out proportional to $\tanh(\overline{h}_x)\,\tanh(\overline{h}_y)$ with $\overline{h}_x \equiv \sum_{z\in C_x} h(z)|\vec{\phi}(z)\cdot\vec{r}|$ (and analogously for $\overline{h}_y$) where $h(z)$ is the local magnetic field, Eq.(14). Clearly such an estimator does not improve the calculation since it can take any sign and moreover it requires a double sum on clusters which makes the necessary computer time exceedingly large.
[43] I. Affleck and F. D. M. Haldane, Phys. Rev. B **36**, 5291 (1987); I. Affleck, D. Gepner, H. J. Schulz and T. Ziman, J. Phys. A **22**, 511 (1989), (Erratum: ibid. A **23**, 4725 (1990)).
[44] G. Bhanot and F. David, Nucl. Phys. **B251**, 127 (1985).